EPJ manuscript No.
(will be inserted by the editor)

Hydrodynamics of DNA confined in nanoslits and nanochannels

Kevin D. Dorfman[1a], Damini Gupta[1], Aashish Jain[1], Abhiram Muralidhar[1], and Douglas R. Tree[1,2]

[1] Department of Chemical Engineering and Materials Science, University of Minnesota – Twin Cities, 421 Washington Ave. SE, Minneapolis, MN 55455 USA
[2] Materials Research Laboratory, University of California – Santa Barbara, Santa Barbara, CA 93106 USA

Abstract. Modeling the dynamics of a confined, semiflexible polymer is a challenging problem, owing to the complicated interplay between the configurations of the chain, which are strongly affected by the length scale for the confinement relative to the persistence length of the chain, and the polymer-wall hydrodynamic interactions. At the same time, understanding these dynamics are crucial to the advancement of emerging genomic technologies that use confinement to stretch out DNA and "read" a genomic signature. In this mini-review, we begin by considering what is known experimentally and theoretically about the friction of a wormlike chain such as DNA confined in a slit or a channel. We then discuss how to estimate the friction coefficient of such a chain, either with dynamic simulations or via Monte Carlo sampling and the Kirkwood pre-averaging approximation. We then review our recent work on computing the diffusivity of DNA in nanoslits and nanochannels, and conclude with some promising avenues for future work and caveats about our approach.

1 Introduction

The properties of DNA molecules confined in either a slit or a channel have received substantial attention in recent years [1–3], combining a seemingly straightforward polymer physics problem with important applications in biotechnology. In this mini-review, we focus on two results that were discussed at the 2014 Max-Planck Workshop on Brownian Motion in Confined Geometries, one solely from our group [4] and another [5] from a collaboration with Patrick Doyle at MIT. These results concern the friction (or, equivalently, the diffusivity) of a long molecule of confined DNA. We particularly emphasize the connection between the configuration of the confined chain, which is affected by the degree of confinement, and the hydrodynamic interactions between segments of the chain and between the chain and the wall. We also take the opportunity to provide the reader with some of the relevant background on DNA in confinement, the experimental data that motivated our studies, and the methodology for computing the diffusion coefficient of a confined DNA molecule.

[a] e-mail: dorfman@umn.edu

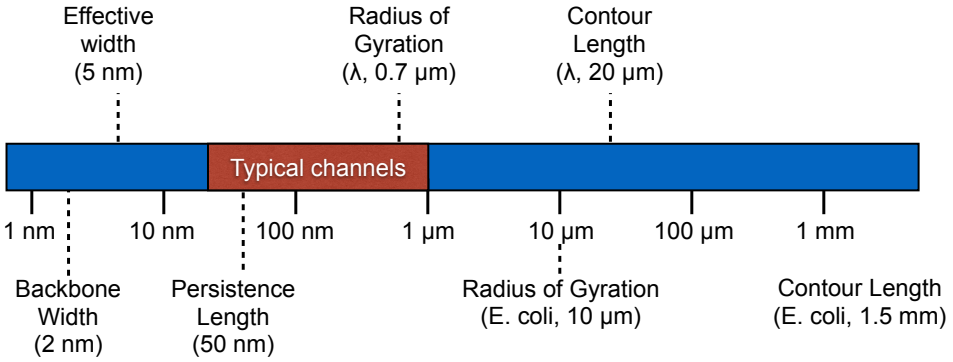

Fig. 1. Typical length scales for the backbone width, effective width, persistence length, radius of gyration, and contour length of λ-DNA and linearized *E. coli* DNA in a high ionic strength buffer. The slits and channel length scales typically range from sub-persistence length (strong confinement, 30 nm) to the radius of gyration (weak confinement, 1000 nm for λ-DNA).

The challenge in describing the dynamic properties of a confined wormlike chain like DNA lies in the length scales characterizing the problem, illustrated in Fig. 1. While the backbone of the DNA has a bare width of around 2 nm, DNA is highly charged in solution due to dissociation of protons from the phosphate groups. Most DNA experiments take place in a reasonably high ionic strength buffer, equivalent to around 100 mM of monovalent salt, where electrostatic interactions are screened over long distances. In such circumstances we typically refer to an "effective width" w of the backbone that maps the interactions between charged segments of DNA to an equivalent neutral polymer. Using the theory by Stigter [6,7], we find this width is approximately 5 nm in a high ionic strength buffer [8–10]. The persistence length of double stranded DNA in a high ionic strength buffer, $l_p = 50$ nm [11], is an order of magnitude higher than the effective width. One often also refers to the Kuhn length, $b = 2l_p$, as a typical length scale for bending.

We can treat the ratio of the Kuhn length to effective width, b/w, as a measure of the monomer anisotropy at a length scale where we view the coarse-grained "monomers" of the chain as the amount of polymer comprising a Kuhn length [10]. DNA is weakly anisotropic; while flexible synthetic polymers such as polyethylene have ratios $b/w \approx 1$, other wormlike polymers such as actin have $b/w \gg 1$. Perhaps the best example of a highly anisotropic wormlike macromolecule is a carbon nanotube, where the persistence length is tens of microns and the width is less than a nanometer [12]. The weak monomer anisotropy of DNA substantially complicates efforts to model its properties in confinement — DNA is sufficiently anisotropic that we need to be concerned about its stiffness, but it is not so stiff that we can treat it locally like a rod. Both the persistence length [13] and the effective width [7] are affected by electrostatic interactions, which can be tuned by changing the ionic strength of the buffer. Note that both quantities vary differently with ionic strength, with the rather counter-intuitive effect that DNA becomes *more* isotropic (decreasing b/w) as it becomes stiffer (increasing b) [10].

We are interested here only in rather long molecules of DNA containing many persistence lengths, which introduces two more length scales much larger than l_p: (i) the radius of gyration, R_g, of the coiled polymer in free solution and (ii) its contour length, L. The "hydrogen atom" of single molecule DNA biophysics is the λ-phage virus genome, often simply called λ-DNA. This molecule has 48,502 base

pairs and it is readily available at high concentrations, making it easy for intrepid physicists to adopt for their own work. The radius of gyration, R_g, of λ-DNA is around 700 nm [14], although the assumptions underlying this analysis have been called into question recently [10, 15]. When λ-DNA is stained with a fluorescent dye for visualization, its contour length L is approximately 20 μm. Note that the actual contour length of stained DNA depends on the dye:base pair ratio and the sample preparation [16].

One of the most attractive features of DNA, aside from its easy visualization by fluorescence microscopy, is its availability in a vast range of molecular weights, all of which are monodisperse due to their biological origin. This means that the possible values of R_g and L span a very wide range, provided the DNA can be handled without breakage [17, 18]. For example, let us consider a linearized form of the *E. coli* genome and extrapolate from the aforementioned estimates for λ-DNA using excluded volume scaling for the radius of gyration, $R_g \sim N_{bp}^{\nu}$, and linear scaling for the contour length, $L \sim N_{bp}$, where N_{bp} is the number of base pairs and $\nu = 3/5$ is the classical value of the Flory exponent. As illustrated in Fig. 1, we thus expect the free solution coil of *E. coli* DNA to be around 10 μm in radius and the entire, stained chain to be 1.5 mm long. In what follows, we will use the classical value of the Flory exponent to keep the mathematics simple, but we should note that the most accurate value of the Flory exponent to date is $\nu = 0.587597(7)$ [19].

The extent of confinement is generally expressed as a ratio of the channel size or slit height relative to the length scales in Fig. 1. Let us rather liberally define a nanochannel or nanoslit as any device with a confining length scale H below 1 μm and focus on the case of λ-DNA. On the upper end of the range of channel sizes in Fig. 1, we have a weak confinement regime, $H \approx R_g$. DNA injected into such a channel will be somewhat deformed into either a pancake shape (in a slit) or a cigar shape (in a channel), as described by de Gennes [20, 21], but the overall size of the chain is not substantially larger than in the bulk. However, as the confinement increases, the chain becomes increasingly stretched in the unconfined directions. For slit-like confinement, the stretching of the chain is measured by the in-plane radius of gyration or the in-plane end-to-end distance. For channel confinement, the stretching is measured by the fractional extension, X/L. In very strong confinement, where $H \ll l_p$, Odijk's theory [22] predicts almost complete extension of the chain in a channel, $X/L \approx 1$. For slitlike confinement, the chain configuration in the Odijk regime corresponds to a random walk of deflection segments whose root-mean square end-to-end distance is described by a modification of the two-dimensional Kratky-Porod model to account for the dependence on the slit height [23]. Since the persistence length and the effective width are controlled, in part, by the ionic strength of the medium, low ionic strength buffers lead to increased stretching of confined DNA for the same value of H [8,24–26].

The strong stretching of DNA in confinement provides a useful approach for genomic mapping, a biological method for obtaining large-scale genomic information. As seen in Fig. 2, this method [25, 30–32] involves inserting sequence specific probes into long pieces of DNA, typically in the hundreds of kilobase pair range, where the probe density is approximately one probe per 5 kilobase pairs. The resulting DNA molecule is sometimes referred to as "barcoded" since the locations of these probes are a unique signature of the genetic information. Injecting the barcoded DNA into a small channel stretches it out from the coiled conformation, allowing the physical distance between probes to be read by fluorescence microscopy. If we also know the fractional extension caused by the confinement, we can convert the physical distance into a genomic distance between barcodes, which is the desired information. There are now a number of reports of genome mapping using nanochannel confinement [27, 33–35], and readers interested in a better understanding of the biotechnology are referred to several excellent, recent reviews on the topic by Ebenstein and coworkers [31, 32].

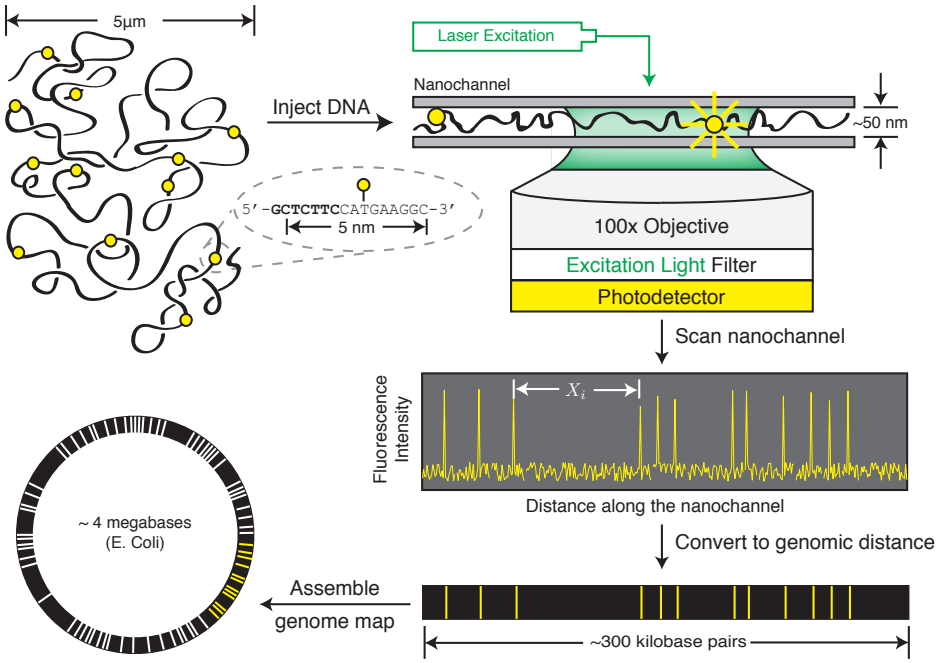

Fig. 2. Principle of genome mapping in nanochannels [25,27]. Long genomic DNA fragments, in the hundreds of kilobase pair range, are decorated with sequence specific probes. As seen in the inset, the nick extension protocol [27] inserts fluorescently labeled nucleotides immediately downstream from the bolded sequence. The DNA is then injected into a nanochannel and stretches along the channel axis. The figure only shows a small ($\approx$ 750 nm) section of the nanochannel. The fluorophores on the labeled nucleotides are excited by laser-induced fluorescence and detected. In practice, the backbone is also fluorescently labeled with a second color (e.g., green) [25,27] to provide a more accurate measurement of the number of base pairs between the fluorescent labels. The measurement of the fluorescence intensity along the nanochannel provides the distance X_i between each of the barcodes. Obtaining multiple measurements on the fluctuating chain reduces the error in the average distance [28]. The linear distances are converted to genomic distances, providing the DNA barcode. Many overlapping DNA barcodes are obtained from different fragments of genomic DNA. The barcodes are then aligned onto the genome, providing the genomic map. In this particular example, the genome size is typical for *E. coli*, but genome mapping has been used for many organisms [3] including humans [27, 29].

The hydrodynamics of confined DNA play a critical role in genome mapping technology. The data for genome mapping are acquired by fluorescence microscopy. When we take an image of the chain, we would like to have an accurate measure of the location of each barcode in the channel. However, the chain is fluctuating under thermal energy. For a dumbbell model, the time scale characterizing these fluctuations of parts of the chain, known as the relaxation time, is given by the ratio of the friction coefficient to the effective spring constant [36]. The effective spring constant is a thermodynamic quantity, which is (relatively) easily obtained through Monte Carlo simulations of the chain configurations. The friction coefficient is a considerably harder quantity to estimate, given that it depends on both the chain configuration and the hydrodynamics in a confined geometry. This harder problem is the subject of our mini-review.

2 Experimental Tests of Blob Theory

With the advances in microfabrication technologies, it is now possible to fabricate channels and slits with well defined geometries and characteristic dimensions ranging from hundreds of nanometers down to the 50 nm length scale corresponding to the persistence length of DNA. This has allowed a direct visualization of confined DNA using epifluorescence microscopy and to investigate the ability of theories to accurately predict the properties of polymers under confinement. As such, the focus of this section will be to cover what is known experimentally about the dynamic properties in nanoslit and nanochannel confinement [37–48] and how these results compare to the classic theory for the dynamics of a confined chain [49].

In order to put our discussion into focus, we first need to recall the blob theory results from Brochard and de Gennes [49]. We denote by H the size of the confinement, either the slit height or the channel width. For both slit and channel confinement, the Brochard and de Gennes blob theory comprises of the following assumptions: (i) The blob size is equal to the confinement size, H, where the conformation of the chain inside a blob is given by that of a three-dimensional, self-avoiding coil in good solvent conditions such that the blob size is $H \sim N_{\rm blob}^{\nu}$, where $N_{\rm blob}$ is the number of persistence lengths inside the blob; (ii) Each blob is a hydrodynamically isolated object such that total friction on each blob is $\zeta_{\rm blob} \sim \eta H$, where η is the viscosity of the fluid; (iii) The blobs themselves form 2D and 1D self-avoiding walks in slits and channels respectively. In other words, the chain is renormalized into a series of blobs that undergo a self-avoiding random walk in a particular dimension. Although the 1D walk implies that this "chain of blobs" is fully extended in a channel, each blob consists of a coiled portion of the original chain. As a result, the polymer itself is not fully extended. The theory applies for relatively weak confinement for channel sizes larger than $H \gtrsim l_p^2/w$ [50].

The theoretical analysis proceeds by first computing the number of persistence lengths in a blob,

$$N_{\rm blob} \sim H^{5/3} w^{-1/3} l_p^{-4/3}, \tag{1}$$

where we use the classical Flory exponent $\nu = 3/5$ for convenience and add the standard corrections for a wormlike chain [51]. The total number of blobs $n_{\rm blob} = N/N_{\rm blob}$, where $N = L/l_p$ is the number of persistence lengths in a chain of contour length L. The total friction on the chain is given by the sum of the friction on all the blobs,

$$\zeta \simeq n_{\rm blob}\zeta_{\rm blob} \sim \eta L \left(\frac{w l_p}{H^2}\right)^{1/3}. \tag{2}$$

The in-plane (slit) and axial (channel) diffusion coefficient of a long chain is thus given by

$$D \equiv \frac{k_B T}{\zeta} \sim \frac{k_B T}{\eta L}\left(\frac{H^2}{w l_p}\right)^{1/3}, \tag{3}$$

where k_B is the Boltzmann constant and T is the absolute temperature. Thus, the scaling of the diffusion coefficient of confined chains in both slits and channels in the de Gennes regime is identical. Note, however, that the scaling of the size of the chain is different in the two cases [21] since the size of a 2D self-avoiding walk of blobs in a slit is different than the size of the 1D self-avoiding walk in a channel. In slits, the in-plane end-to-end distance can be written as

$$R \simeq (n_{\rm blob})^{3/4} H \sim L^{3/4}\left(\frac{w l_p}{H}\right)^{1/4}, \tag{4}$$

while the extension in channels is given by

$$X \simeq (n_{\text{blob}})H \sim L\left(\frac{wl_p}{H^2}\right)^{1/3}. \tag{5}$$

The size of a confined DNA chain, at least in the range of confinement satisfying the blob model, is now a relatively settled question. In slits, the scaling in Eq. (4) was first demonstrated experimentally [44] for λ-DNA using slit heights $2 < R_g/H < 8.4$ and subsequently confirmed by a number of studies [45, 47, 48]. Note that Ref. [44] also reports a sharp transition in the extension at $H \approx l_p$, which has been repeatedly criticized [46]. In nanochannels, the seminal experiments on DNA confinement in nanochannels by Reisner *et al.* [38] used one channel size in the strong confinement limit ($H < l_p$) and six channel sizes in the weak confinement limit ($l_p < H < R_g$). The experimental extension data in the weak confinement limit were fit by $X \sim H^{-0.85}$, a stronger dependence on H than originally anticipated by Eq. 5. The origin of this unexpected behavior is now understood to be due to the presence of a broad transition regime between the limiting cases of weak and strong confinement [9, 10, 50, 52].

The situation surrounding the diffusivity in Eq. 3 is considerably less clear. The earliest studies for DNA diffusion in slits [37, 39] probed this scaling result by measuring the diffusivity of a number of different chains of size L in channels of different size H. If the chains are sufficiently long, then their diffusivity in the bulk should be Zimm-like and thus scale inversely with their hydrodynamic radius. The latter quantity is usually assumed to be proportional to the radius of gyration, leading to $D_{\text{bulk}} \sim R_g^{-1}$. If blob theory is correct, then a plot of D/D_{bulk} vs R_g/H should yield a universal curve, independent of molecular weight, with a scaling exponent of $-2/3$ [37, 39]. These early experimental studies [37, 39] indeed found a good collapse of the data obtained from different molecular weights with the expected scaling exponent. However, a closer look at the data [40] revealed that the spread of the band of the collapsed data is larger than the uncertainty in the experimental measurements.

The origin of this discrepancy was not clear. One possibility is that the blob theory is incorrect or even that the free solution diffusivity does not scale inversely with the radius of gyration for these DNA sizes, which may be a distinct possibility [10, 15]. Alternatively, there may be a systematic deviation in the experimental data. The limitations of the blob theory became more clear by measuring D as a function of chain length L for fixed values of the slit height H from 190 nm to 545 nm [40]. These experiments revealed a scaling exponent ranging from $L^{-0.85}$ to $L^{-0.95}$ [40] indicating that the blobs might not be hydrodynamically isolated and interact at a length scale larger than H [40–43]. However, the scaling of D with H was found to be slightly weaker than the expected result $D \sim H^{2/3}$ from blob theory. The experimental data for λ-DNA were fit by $D \sim H^{0.55}$ [40], $D \sim H^{0.48}$ [41], $D \sim H^{0.49}$ [46] and $D \sim H^{0.56}$ [48] for slit height range $2l_p < H < R_g$. Additionally, the scaling $D \sim H^{0.52}$ [43, 46] extended down to slit heights lower than l_p indicating that the onset of the Odijk regime is gradual. The origin of this weaker dependence of D on H will be the focus of the discussion in Section 4.1.

No experimental data exist for the axial diffusion coefficient of a DNA molecule in nanochannels. However, measuring the relaxation time provides an indirect tool to analyze the hydrodynamics of a channel-confined chain. Reisner *et al.* [38] observed a sharp non-monotonic transition in the relaxation time τ for a channel size $H \approx 2l_p$. Section 4.2 will be directed towards elucidating this sharp transition of τ in the channel size of the order of $2l_p$ through a deeper understanding of the friction in these channel sizes.

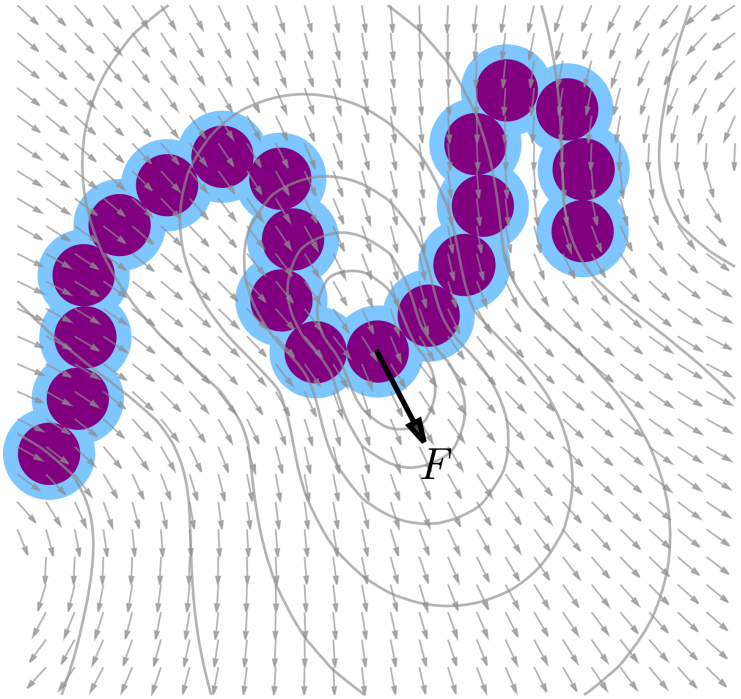

Fig. 3. Schematic of hydrodynamic interactions for a discrete polymer chain. A point force is applied to one of the beads and the resulting flow field affects the dynamics of the rest of the chain.

3 Hydrodynamic interactions

It has been our contention that the simplistic treatment of hydrodynamic interactions in blob theory is the reason for the discrepancy between theory and experiments in slits [5], and even more important if we want to understand DNA diffusion in nanochannels [4]. To be more precise, the movement of polymer segments in a fluid affect the velocities of other segments through fast diffusive momentum transport. These hydrodynamic interactions (HI) play a vital role in the dynamics of polymer solutions [53]. Figure 3 depicts the role of HI on the collective dynamics of the chain. Here, one part of the chain is perturbed by a force **F** and induces a flow in the solvent. This flow is long-ranged and entrains other parts of the chain by an induced drag force. Thus, HI are solvent mediated intrachain interactions between distal segments of the chain and are the dynamic analogue of excluded volume. The HI is long-ranged in free solution. However, it changes dramatically in confined domains owing to the need to satisfy no-slip and no-penetration at the channel walls, resulting in a significant change in the polymer dynamics [54–59].

The underlying assumption in blob theory is that there are sufficient hydrodynamic interactions inside a blob to lead to non-draining behavior, whereupon $\zeta_{\text{blob}} \sim \eta H$, but that the walls *completely* screen any hydrodynamic interactions between blobs. We [4, 5] are not the first to express concern about these hydrodynamic approximations [37,40,46,54,60,61], as the concept of screening is more subtle than it was initially perceived [49]. For channels, the HI is known to decay exponentially [62–64]. However, the decay in slits is only algebraic [5, 62, 65]. Therefore it is not entirely obvious that hydrodynamic screening leads to $\zeta \sim L^1$ in slits. Doyle and

coworkers argued that it is the coupling between the configuration and the hydrodynamic interactions in the long-chain limit that determines the scaling of ζ with L [40, 66]. In fact, their analysis showed that $\zeta \sim L(\ln L)^{-1}$ for ideal chains in slits, indicating partial draining of blobs [40]. This result was later substantiated theoretically via the pre-averaging approximation [67]. Nonetheless, Doyle and coworkers [40] found that, for slit-confined polymers in good solvent conditions, ζ is indeed proportional to L, in agreement with the somewhat fortuitously obtained outcome of blob theory, where the hydrodynamic interactions were assumed to decay exponentially outside of a distance H for both channels and slits [49].

For channels, Harden and Doi [60] estimated the prefactor for the scaling of D in Eq. 3 for flexible polymers. By using a combination of the Kirkwood approximation and self-consistent field theory, they claimed that $D \sim H^{0.61}$, slightly weaker than the scaling in Eq. 3. However, it remains to be seen whether this prediction is correct, considering that mean-field theory overestimates the effect of self-avoidance on monomer distribution in channel confinement [68].

To address the role of hydrodynamic interactions, amongst other things, Kirkwood and Riseman developed a formalism treating the solvent as an implicit continuum, leaving only the polymer degrees of freedom [69–72]. These degrees of freedom are expressed in terms of the coordinates $\mathbf{r}_i$ of the N_b beads that are used to represent the polymer chain. The Kirkwood-Riseman approach can be expressed quite generally as a Fokker–Planck equation for the time evolution of the probability density of the chain configuration [53],

$$\frac{\partial \psi}{\partial t} = \sum_{i=1}^{N_b} \sum_{j=1}^{N_b} \frac{\partial}{\partial \mathbf{r}_i} \cdot \mathbf{D}_{ij} \cdot \left[\frac{\partial \psi}{\partial \mathbf{r}_j} + \frac{\psi}{k_B T} \frac{\partial H}{\partial \mathbf{r}_j} \right], \tag{6}$$

where $\mathbf{D}_{ij}$ is a 3×3 diffusion tensor and H is the Hamiltonian describing the configuration-dependent potential field acting on the chain. One of the distinguishing features of Eq. 6 is its capacity to incorporate hydrodynamic interactions (HI), which are a crucial part of correctly modeling polymer dynamics. However, it is important to recognize that HI are a dynamic effect only. Because the time-averaged force on the polymer from the solvent is zero, HI do not alter ψ in the long time limit.

Hydrodynamic interactions enter Eq. 6 through the diffusion tensor. To find this tensor, consider the change in velocity of the solvent, $\mathbf{v}_i$, from a quiescent state, due to the drag $\mathbf{F}_i$ acting on a given segment i of the chain. The velocity is thus the disturbance flow caused by all N_b of these forces,

$$\mathbf{v}_i = \sum_{j=1}^{N_b} \mathbf{\Omega}_{ij} \cdot \mathbf{F}_j, \tag{7}$$

where the hydrodynamic interaction tensor $\mathbf{\Omega}_{ij}$ accounts for the flow at bead i caused by the force acting on each bead $j \neq i$. This quantity is the Green's function of the Stokes equation, and it depends on the boundary conditions. We will discuss how to calculate the hydrodynamic interaction tensor at length in Section 3.1. For the moment, we simply assume that it is a computable quantity. The drag force is given by the product of the bead friction coefficient, ζ, and the difference between the bead velocity $\mathbf{u}_i$ and the solvent velocity,

$$\mathbf{F}_i = \zeta \left(\mathbf{u}_i - \mathbf{v}_i \right). \tag{8}$$

Substituting Eq. 7 into Eq. 8 gives

$$\mathbf{F}_i = \zeta \mathbf{u}_i - \zeta \sum_{j=1}^{N_b} \mathbf{\Omega}_{ij} \cdot \mathbf{F}_j, \tag{9}$$

which is a self-consistent equation for the drag force in terms of the bead velocities and the hydrodynamic tensor. Defining the diffusion tensor according to the fluctuation-dissipation theorem

$$\mathbf{u}_i = \frac{1}{k_B T} \sum_{j=1}^{N_b} \mathbf{D}_{ij} \cdot \mathbf{F}_j \tag{10}$$

and rearranging Eq. 9 yields the sought-after expression

$$\mathbf{D}_{ij} = k_B T \left(\frac{\delta_{ij}}{\zeta} \mathbf{I} + (1 - \delta_{ij}) \mathbf{\Omega}_{ij} \right), \tag{11}$$

where δ_{ij} is the Kronecker delta function. It is worth noting that in the general formulation of the Kirkwood–Riseman theory, Eq. 11 is not exact when constraints on the system (e.g. rigid bond angles) are included [73]. In this case, Eq. 11 only represents the first two terms in an expansion in the strength of the hydrodynamic interactions [74].

3.1 Computing the Hydrodynamic Interaction Tensor

In free solution, the hydrodynamic interaction tensor $\mathbf{\Omega}_{ij}$ is the 3×3 Oseen–Burgers tensor from the solution of the Stokes equation due to a point force perturbation [53],

$$\mathbf{\Omega}_{ij} = \frac{1}{8\pi\eta r_{ij}} \left(\mathbf{I} + \frac{\mathbf{r}_{ij}\mathbf{r}_{ij}}{r_{ij}^2} \right) \text{ for } i \neq j. \tag{12}$$

In Eq. 12, $\mathbf{r}_{ij}$ is the distance vector $\mathbf{r}_j - \mathbf{r}_i$, the magnitude of this distance vector is r_{ij} and η is the solvent viscosity. The Oseen–Burgers tensor becomes non-positive definite for overlapping particles. In the context of the touching bead model of DNA, which we use frequently for dynamics studies [4, 10, 75], each hard bead has a size equal to the effective width of the DNA. The rod connecting two beads represents a small amount of polymer and thus has a small hydrodynamic radius, so bead-bead hydrodynamic overlap is not possible. For bead-spring models, where the bead-bead interaction potentials are soft and each spring represents a substantial amount of polymer and thus has a larger hydrodynamic radius than a touching bead, the bead overlap is a potential problem. This problem is overcome in bead-spring models by replacing the Oseen-Burgers tensor by the Rotne-Prager-Yamakawa (RPY) tensor, which is a regularized version of the Oseen–Burgers tensor [76–79].

The need to satisfy no-slip and no-penetration at the channel walls substantially increases the difficulty in obtaining $\mathbf{\Omega}_{ij}$ for a confined chain. Jendrejack *et al.* [54] developed a numerical scheme to calculate the HI tensor $\mathbf{\Omega}$ by splitting it into two parts,

$$\mathbf{\Omega} = \mathbf{\Omega}^{\mathrm{F}} + \mathbf{\Omega}^{\mathrm{W}}, \tag{13}$$

where $\mathbf{\Omega}^{\mathrm{F}}$ is the free-space HI tensor and $\mathbf{\Omega}^{\mathrm{W}}$ is a correction tensor that accounts for the presence of the walls through no-slip conditions. The velocity perturbation due to a point force acting at $\mathbf{r}_j$ is $\mathbf{u} = \mathbf{\Omega}(\mathbf{r}, \mathbf{r}_j) \cdot \mathbf{F}(\mathbf{r}_j)$, which is also the summation of the velocity perturbations due to $\mathbf{\Omega}^{\mathrm{F}}$ and $\mathbf{\Omega}^{\mathrm{W}}$, respectively. The velocity perturbation

$$\mathbf{u}_{\mathrm{W}} = \mathbf{\Omega}^{\mathrm{W}}(\mathbf{r}, \mathbf{r}_j) \cdot \mathbf{F}(\mathbf{r}_j) \tag{14}$$

due to the wall correction part is obtained by solving the incompressible Stokes equation

$$\begin{aligned} -\nabla p + \eta \nabla^2 \mathbf{u}_{\mathrm{W}} &= 0, \\ \nabla \cdot \mathbf{u}_{\mathrm{W}} &= 0 \end{aligned} \tag{15}$$

Fig. 4. Velocity profile generated due to a point particle located at $\mathbf{r}_i = (0, 0, 0)$ exerting a point force f_i in the y-direction on the solvent in a channel of aspect ratio $L_x/L_y = 10$. Here, L_x is the length and L_y is the width of the simulation cell.

subject to the no-slip boundary condition

$$\mathbf{u}_{\mathrm{F}} + \mathbf{u}_{\mathrm{W}} = 0 \quad \text{at the walls,} \tag{16}$$

where $\mathbf{u}_{\mathrm{F}} = \mathbf{\Omega}^{\mathrm{F}}(\mathbf{r}, \mathbf{r}_j) \cdot \mathbf{F}(\mathbf{r}_j)$ is the velocity perturbation due to $\mathbf{\Omega}^{\mathrm{F}}$. An example of the flow generated by a point force is shown in Fig. 4.

The calculation of $\mathbf{\Omega}^{\mathrm{F}}$ is straightforward as analytical expressions are known, such as the Oseen-Burgers tensor in Eq. 12. However, calculating the tensor $\mathbf{\Omega}^{\mathrm{W}}$ is not trivial. It was first calculated by Jendrejack *et al.* [54] using the finite-element method. First, a free-solution velocity perturbation field $\mathbf{u}_{\mathrm{F}}(\mathbf{r}-\mathbf{r}_j)$ is calculated at the walls by considering a point particle at $\mathbf{r}_j$ which acts in x-direction with a point force f_1. Using numerical values of $\mathbf{u}_{\mathrm{F}}(\mathbf{r} - \mathbf{r}_j)$ at the walls, we solve Eq. (15) numerically to obtain $\mathbf{u}_{\mathrm{W}}(\mathbf{r}, \mathbf{r}_j)$. The first column of $\mathbf{\Omega}^{\mathrm{W}}$ is then obtained by

$$\begin{pmatrix} \Omega^{\mathrm{W}}_{11} \\ \Omega^{\mathrm{W}}_{21} \\ \Omega^{\mathrm{W}}_{31} \end{pmatrix} = \frac{1}{f_1} \mathbf{u}_{\mathrm{W}}. \tag{17}$$

The second and third columns of $\mathbf{\Omega}_{ij}$ are obtained similarly by applying the point forces in y and z-directions, respectively. Finally, $\mathbf{\Omega}_{ij}$ is calculated using

$$\mathbf{\Omega}_{ij} = \mathbf{\Omega}^{\mathrm{W}}(\mathbf{r}_i, \mathbf{r}_j) + (1 - \delta_{ij})\, \mathbf{\Omega}^{\mathrm{F}}(\mathbf{r}_i - \mathbf{r}_j). \tag{18}$$

It is important to note that $\mathbf{\Omega}_{ij}$ is nonzero for $i = j$ in confinement, while in free-solution it is zero.

In order to solve the Stokes equation, and hence to calculate $\mathbf{\Omega}^{\mathrm{W}}(\mathbf{r}_i, \mathbf{r}_j)$, a grid is generated in a predefined geometry. At first glance, it would appear that we need to compute $\mathbf{\Omega}^{\mathrm{W}}(\mathbf{r}_p, \mathbf{r}_q)$ for all pairs of p and q, where p and q are grid indices. However, we can perform such calculations in an efficient manner by making use of the fact that hydrodynamic interactions decay rapidly in confined geometries. In other words, we can calculate $\mathbf{\Omega}^{\mathrm{W}}(\mathbf{r}_p, \mathbf{r}_q)$ for only those pairs of p, q such that $|\mathbf{r}_{pq}| < r_c$, where $|\mathbf{r}_{pq}|$ is distance between grid points p and q, and r_c is the cutoff distance which depends on the size of the channel or height of the slit. Since we have a grid, an interpolation procedure is used on the grid to obtain $\mathbf{\Omega}^{\mathrm{W}}(\mathbf{r}_i, \mathbf{r}_j)$ for real particle locations. We can further reduce the size of the calculation by taking advantage of any symmetries in the channel geometry.

3.2 Brownian Dynamics

In principle, once we know how to compute $\mathbf{D}_{ij}$, we could solve Eq. 6 directly for the center of mass diffusion coefficient. Unfortunately, this is an intractable problem for a chain with so many degrees of freedom [36, 80]. Accordingly, a number of approximations are commonly made to arrive at a concrete prediction for the diffusivity. The

most mild of these involves a straightforward numerical solution. The numerical calculations are performed by reformulating Eq. 6 in terms of a set of coupled stochastic differential equations and integrating in time akin to Molecular Dynamics [79, 80]. Such calculations are commonly referred to as Brownian Dynamics simulations (with hydrodynamics) and can be computationally quite expensive.

In Brownian Dynamics (BD), the explicit solvent particles are replaced by stochastic forces. The BD method is based on a large separation of time scales between the rapid motion of solvent particles and the more sluggish motion of polymer segments, making it useful for problems where the details of the structure of the polymer, but not the fluid, are of interest. The idea is to make an analogy between a Fokker-Planck equation for the probability density of random variables and Ito stochastic differential equations (SDE) for these random variables [80]. For a bead-spring chain consisting of N_b beads and $N_s = N_b - 1$ springs, the dynamics are described by an Ito-Euler stochastic differential equation

$$d\mathbf{r} = \left[\frac{1}{k_B T}\mathbf{D}\cdot\mathbf{F} + \frac{\partial}{\partial \mathbf{r}}\cdot\mathbf{D}\right]dt + \sqrt{2}\mathbf{B}\cdot d\mathbf{W}, \tag{19}$$

where $\mathbf{r}$ is a vector containing the $3N_b$ coordinates of the beads that constitute the polymer chain, with $\mathbf{r}_i$ denoting the Cartesian coordinates of bead i. The vector $\mathbf{F}$ is the sum of non-Brownian and non-hydrodynamic forces, which has length $3N_b$, with $\mathbf{F}_i$ denoting the force acting on bead i. The components of the Gaussian noise $d\mathbf{W}$ are obtained from a real-valued Gaussian distribution with zero mean and variance dt. The quantity $\mathbf{B}$ is a tensor whose presence leads to multiplicative noise [80]. Its evaluation requires the decomposition of the diffusion tensor using the fluctuation-dissipation theorem, $\mathbf{D} = \mathbf{B}\cdot\mathbf{B}^T$.

Apart from calculating the HI tensor, which appears in Eq. 19 through Eq. 11, there are two more terms in Eq. 19 that are difficult to calculate, namely the stochastic term $\mathbf{B}\cdot d\mathbf{W}$ and the divergence term $\partial/\partial\mathbf{r}\cdot\mathbf{D}$, which is non-zero in confinement due to the HI. For the stochastic term, the Chebyshev polynomial approximation [81] or the Krylov subspace method [82] can be used. A recent paper by Saadat and Khomami [83] compares different methods to compute the stochastic term. The divergence term can be handled efficiently by using the mid-point algorithm [84,85]. The BD algorithm from Jendrejack *et al.* [54, 79] carries out the calculation of both terms in a matrix free manner proposed by Fixman [81], which results in a $\mathcal{O}\left(N_b^{2.25}\right)$ CPU time scaling. While this approach is useful for relatively small systems and has a favorable prefactor, the N_b scaling eventually becomes unfavorable for a large number of beads.

The method described above is but one approach to calculate the hydrodynamic interactions in BD simulations of polymers in confinement. A method developed by Mucha *et al.* [86] was generalized by Hernández-Ortiz *et al.* [87] to calculate the velocity perturbations due to point particles. The computational time of this method scales as $\mathcal{O}\left(N_b^{1.66}\right)$, where N_b is the number of beads in the polymer model, which exert point forces on the solvent. However, it is restricted to slit geometries only. In order to have a better scaling and solve problems with arbitrary geometries, Hernández-Ortiz *et al.* [88] developed a method called the General Geometry Ewald-like Method (GGEM). In GGEM, the point force density is split into two parts: (i) the local force density and (ii) the global force density. The local force density drives a local velocity field, which is solved analytically by assuming an unbounded domain. The global force density causes a global velocity field, which is calculated through suitable numerical approaches. For example, for slit geometries, where one direction is in confinement and the other two directions are considered to be periodic, $\mathcal{O}\left(N_b \log N_b\right)$ scaling is obtained by using fast Fourier transform (FFT) in the periodic directions [88]. For channels, and other geometries in which more than one direction is non-periodic, FFT

cannot be used in those directions, and rather finite difference, finite volume or finite element methods can be used [89,90] to solve the global velocity field problem. While the scaling for GGEM is very good, the prefactor can be large.

3.3 Kirkwood Pre-Averaging Approximation

As an alternative to an expensive Brownian Dynamics calculation, we could follow Kirkwood and Riseman in making a so-called pre-averaging approximation for the center of mass diffusivity [69,74]. The center of mass diffusion tensor $\mathsf{D}_{\rm cm}$ is defined implicitly as

$$\mathbf{u}_{\rm cm} = \frac{1}{k_B T}\mathsf{D}_{\rm cm} \cdot \mathbf{F}_{\rm cm}, \tag{20}$$

where

$$\mathbf{u}_{\rm cm} = \frac{1}{N_b}\sum_{i=1}^{N_b} \langle \mathbf{u}_i \rangle \tag{21}$$

and

$$\mathbf{F}_{\rm cm} = \sum_{i=1}^{N_b} \langle \mathbf{F}_i \rangle \,. \tag{22}$$

In the latter equations, $\langle \cdots \rangle$ is the ensemble average operator. Summing Eq. 10 over i, dividing by N_b and taking the ensemble average gives

$$\mathbf{u}_{\rm cm} = \frac{1}{N_b k_B T}\sum_{i=1}^{N_b}\sum_{j=1}^{N_b} \langle \mathsf{D}_{ij} \cdot \mathbf{F}_j \rangle \,, \tag{23}$$

which is as far as we can progress without an approximation. The pre-averaging approximation consists in separating $\mathbf{F}_j$ from D_{ij} in the ensemble average

$$\mathbf{u}_{\rm cm} = \frac{1}{N_b k_B T}\sum_{i=1}^{N_b}\sum_{j=1}^{N_b} \langle \mathsf{D}_{ij} \rangle \cdot \langle \mathbf{F}_j \rangle \,, \tag{24}$$

resulting in the well-known Kirkwood double-sum formula [70]

$$\mathsf{D}_{\rm cm} = \frac{1}{N_b^2}\sum_{i=1}^{N_b}\sum_{j=1}^{N_b} \langle \mathsf{D}_{ij} \rangle \,. \tag{25}$$

The pre-averaging approximation in Eq. 24 is essentially a hydrodynamic mean-field approximation, where a chain segment feels the average HI at every point in time. Accordingly, the approximation neglects the dynamic correlations that exist between the intramolecular hydrodynamic interactions at different points in time [91,92]. Because these correlations are also small at short times, the Kirkwood diffusivity in Eq. 25 can be thought of as a short-time diffusion coefficient. Using linear response theory, Fixman [91] showed that dynamic intramolecular correlations always decrease the diffusivity, making the Kirkwood estimate an upper bound to the true diffusivity [92].

An alternative technique called the rigid-rod approximation has been tried in an attempt to overcome the limitations of pre-averaging. In this approach, one numerically solves Eq. 23 using the expression for the drag forces in Eq. 9 before performing

the ensemble average using Monte Carlo data [93]. This technique does indeed circumvent the pre-averaging, but instead assumes that the dynamic correlations are between "rigid" conformations of the polymer. This approach has been questioned theoretically [94], and numerical results yield errors similar or worse than the pre-averaging approximation [95].

4 Kirkwood Approximation Results for the Diffusivity of DNA

Having completed our review of the literature, we now proceed to discuss two results obtained by our group for DNA in nanoslits [5] (with Patrick Doyle) and nanochannels [4]. In both of these studies, we used a Monte Carlo sampling of the pre-averaged Kirkwood approximation in Eq. 25. The DNA chain consists of touching beads of size w with a bending energy [96] to enforce the desired persistence length l_p. We further assumed that the DNA-DNA excluded volume interactions and DNA-wall excluded volume iterations were the same, using a hard core potential of size w. Although we have since developed more sophisticated approaches for computing the chain configurations out to hundreds of thousands of beads [10,97,98], the data we will discuss below were obtained using a Metropolis Monte Carlo algorithm consisting of reptation, crankshaft and pivot moves [9] for around 2000 beads. For slit confinement, the hydrodynamic interactions were obtained from the method of reflections solution [65]. For channel confinement, we obtained the hydrodynamic interaction tensor from the grid-based method of Jendrejack *et al.* [54], using finite differences to compute the wall contribution to the flow.

4.1 Nanoslits (Based on Ref. [5])

As we noted in our discussion of the experimental data, the in-plane size of a DNA molecule contained in a slit of height H exhibits the expected scaling with respect to the slit height, $R \sim H^{1/4}$. However, as we can see in Fig. 5(a), the simulation data for the diffusivity agree with the trends seen in experiments [40, 43, 46] and, as a result, do not exhibit classical blob theory scaling $D \sim H^{2/3}$. In this figure, the quantity

$$D_0 = \frac{k_B T}{6\pi\eta L} \tag{26}$$

is the Rouse diffusivity for a chain of length L, which just serves as a convenient normalization factor.

To be more quantitative in the comparison between scaling theory and our simulations, we estimated the apparent power law over the range $2l_p < H < R_g$, which corresponds to the filled symbols in Fig. 5(a). This analysis led to $D \sim H^{0.523}$, which is quite similar to the power laws reported in previous experimental studies [40,43,46]. Note that, for the largest channel sizes in Fig. 5(a), the confinement becomes weak and the diffusion coefficient is transitioning to its bulk value. This transition can be shifted to ever larger values of the channel size by increasing the molecular weight of the polymer, but such an analysis requires moving from a Metropolis Monte Carlo approach to a more sophisticated method [10, 97].

Given that the simulations and experiments were in reasonable agreement, it seems natural to question the theoretical result. To do this, we noted that the pre-averaged Kirkwood approximation in Eq. 25 could instead be written as [20]

$$D = \frac{k_B T}{L} \int_0^{H/2} h(r)\Omega(r)\mathrm{d}r, \tag{27}$$

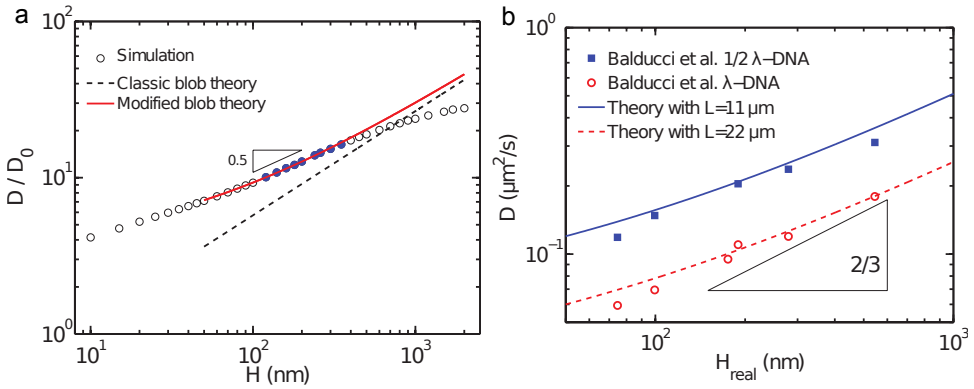

Fig. 5. (a) DNA diffusivity as a function of slit height. The filled circles correspond to the range $2l_p < H < R_g$. The dashed line is Eq. 3. The solid (red) line is Eq. 31. The slit height H in this panel is the amount of the channel available to the hard beads. (b) Comparison between the modified blob theory and experimental data. The symbols are from experiments by Balducci *et al.* [40] for both λ-DNA and 1/2 λ-DNA. The two lines are calculated from Eq. 31. The triangle indicates the scaling in Eq. 3. The slit height H_{real} in this panel is the full height of the slit. Adapted with permission from Ref. [5].

where $h(r) \equiv 4\pi r^2 l_p g(r)$ is a dimensionless form of the pair correlation function and, as an approximation, we could average over the confined hydrodynamic mobility tensor to obtain a form $\Omega(r)$ that only depends on the radial distance between segments. If we go back to the discussion of Section 2 and review it in the context of Eq. 27, we see that the classical blob theory makes two assumptions. First, the hydrodynamic interactions are assumed to be the same as those in free solution for $r < H$. In other words, we can average over Eq. 12 to get

$$\Omega(r) = \frac{1}{6\pi r\eta} \quad \text{for} \quad r < H. \tag{28}$$

Outside the hydrodynamic screening distance H, there are assumed to be no hydrodynamic interactions, which sets the upper bound in the integral in Eq. 27. Second, the classic blob theory assumes that the pair correlation function is equivalent to a flexible polymer in a good solvent inside the blob volume H^3,

$$h(r) \sim r^{2/3}. \tag{29}$$

Using these two assumptions in Eq. 27 yields $D \sim H^{2/3}$, which is the result we got from blob theory in Eq. 3.

The shortcoming of the classical blob theory is the assumption in Eq. 29 that there are no correlations between the segments of the chain inside a blob. Since DNA is a wormlike chain, the orientation of nearby segments along the chain backbone are strongly correlated with one another, only losing the correlations at a contour length $r \approx l_p$. We thus proposed [5] a modified form of the pair correlation function

$$h(r) = \begin{cases} 2 & \text{for } r < l_p/2 \\ 2.8\left(\dfrac{r^2}{l_p w}\right)^{1/3} & \text{for } r \geq l_p/2 \end{cases} \tag{30}$$

that crudely accounts for the correlations over short distances and reduces to the classical blob theory for distances larger than the persistence length. The prefactor of

2.8 for longer distances was obtained by computing the contour length per blob from the simulations and fitting these data to the resulting prediction from Eq. 30.

If we use the modified pair correlation function in Eq. 30 in the expression for the diffusivity in Eq. 27, we obtain a diffusion coefficient

$$\frac{D}{D_0} = 1.68 \left[\left(\frac{H^2}{l_p w} \right)^{1/3} - \left(\frac{l_p}{w} \right)^{1/3} \right] + 2 \ln \left(\frac{l_p}{a} \right) \tag{31}$$

where, in our comparison to experiments in this paper [5], we used $a = 1.38$ nm as the hydrodynamic radius of the beads. We retained an $O(1)$ prefactor for the first term to allow us to approximately correct for the assumptions in the pre-averaging; the best fit curve seen in Fig. 5(a) corresponds to the prefactor 1.68. When we use realistic values for the persistence length, contour length, and effective width [5], Eq. 31 leads to excellent agreement with the experimental data in Fig. 5(b).

4.2 Nanochannels (Based on Ref. [4])

The statics and dynamics of DNA in a nanochannel are qualitatively different than these properties in a slit. In the latter case, the DNA is confined in one direction and thus executes a two-dimensional, self-avoiding random walk of blobs (in the case of weak confinement) or deflection segments (in the case of strong confinement). As we have focused for the most part on the de Gennes blob regime in this mini-review, we should point out that many experiments of DNA confined in nanochannels employ channels whose size is comparable to the persistence length of the molecule [1, 24, 28, 38, 99, 100]. The predictions of blob theory are no longer valid in this limit. For narrower channels corresponding to the Odijk regime ($H \ll l_p$), the diffusion coefficient can be estimated using the expression for motion of a single semiflexible polymer in a tube given by [2, 101]

$$D \simeq \frac{k_B T}{2\pi\eta X} \ln \left(\frac{H}{2a} \right), \tag{32}$$

where a is the hydrodynamic radius of the DNA. The extension of the chain in the Odijk regime [22] also differs from Eq. 5, having the form

$$X = L \left[1 - 0.18274 \left(\frac{H}{l_p} \right)^{2/3} \right], \tag{33}$$

where the prefactor comes from the calculation by Burkhardt *et al.* [102]. Since the chain is almost at full extension, it is common to replace the extension with the contour length in Eq. 32.

In a nanochannel, the DNA is confined in two dimensions and thus executes a self-avoiding walk in one dimension, again corresponding to blobs or deflection segments depending on the nature of the confinement. In both nanoslits and nanochannels, there must be a transition from deflection segments to blobs. The interesting feature of DNA in nanochannel confinement is that the weak monomer anisotropy of DNA leads to this so-called transition regime occupying almost the entire range of measurable extensions in experiments [97], from around 20% to 85% fractional extension. Thus, although the theories for the hydrodynamic friction for the Odijk and de Gennes regimes are well established, they are of little use for describing most experiments involving DNA in nanochannels.

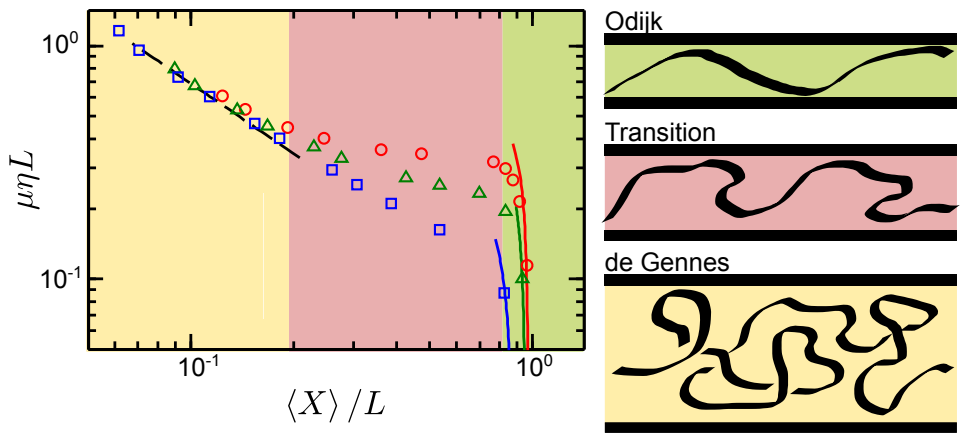

Fig. 6. Hydrodynamic mobility, made dimensionless with the Rouse mobility, as a function of fractional extension of the chain. All simulations correspond to an effective width $w = 4.6$ nm, hydrodynamic radius $a = 1.38$ nm and $L = 9.42$ μm ($N_b = 2048$ beads). The data correspond to three different persistence lengths: 53 nm (red circles), 26 nm (green triangles), and 5 nm (blue squares) The dotted line is the scaling of Eq. 3. The solid lines are the approximation in Eq. 32 with $X = L$. The shaded regions of the plot, along with the corresponding schematics, represent different regimes of confinement. Adapted with permission from Ref. [4].

To understand exactly how the flexibility of a polymer affects its hydrodynamic mobility $\mu \equiv D/k_BT$ in confinement, we fixed the effective width at $w = 4.6$ nm and simulated chains with persistence lengths of 53 nm, which corresponds to DNA, and 5 nm, which is a flexible chain [4]. As we see in Fig. 6, the flexible chain exhibits the scaling predicted by Brochard and de Gennes [49] up to almost complete extension. Thus, we can conclude that a flexible chain is a hydrodynamically non-draining object, where the friction of the chain (inverse of the mobility) is proportional to its size, X. Only when the channel size is almost equal to the width of the chain does this flexible molecule exhibit the lubrication result that we would expect in the Odijk regime. The solid lines in Fig. 6 are Eq. 32 for the Odijk regime with $X = L$, which is an excellent approximation to the simulation data. In contrast, our simulation of a DNA-like model exhibits a broad plateau in the mobility for a wide range of fractional extensions. In this figure, we have made the hydrodynamic mobility μ dimensionless with the characteristic value $\mu_R \sim (\eta L)^{-1}$ of a freely draining (Rouse) chain [53], independent of the extension X. In a freely draining chain, each monomer acts as its own friction center and there are no hydrodynamic interactions. Thus, for most channel sizes where there is a sensible extension of the DNA compared to its bulk conformation, the hydrodynamic interactions between segments of the chain are almost completely screened. It is only at the smallest fractional extensions where we see the DNA hydrodynamic mobility approach the prediction from Brochard and de Gennes [49]. At the highest extensions, we again see a shift to the prediction for the Odijk regime, where the DNA-wall hydrodynamic interactions dominate. To confirm that the freely draining behavior at intermediate extensions is a result of semiflexibility, we also simulated a chain with an intermediate monomer anisotropy ($l_p = 26$ nm) [4]. As we can see in Fig. 6, the trend in the hydrodynamic mobility for $l_p = 26$ nm is between the result for a flexible chain and DNA.

Similar to what we saw for the slit confinement, the trend in the hydrodynamic mobility for channel-confined DNA reflects the coupling between the conformations of the chain and the hydrodynamic interactions, both polymer-polymer and polymer-

wall. There are thus two factors that we need to analyze: (i) the density of polymer inside the hydrodynamic screening volume H^3 and (ii) the typical distance between the polymer and the wall, given by the ratio of the hydrodynamic radius of the beads to the channel size, a/H. In the de Gennes regime, the monomer density is high because the channel size H is big enough to permit backfolding of the chain, thereby enabling the formation of 3D self-avoiding walks within the hydrodynamic screening volume. Moreover, the channel is much larger than the typical hydrodynamic size of the monomers. As a result, we have strong polymer-polymer hydrodynamic interactions and weak polymer-wall interactions, leading to the non-draining hydrodynamic mobility [49]. As the channel size decreases to the transition between the de Gennes and Odijk regimes, which corresponds to $H \approx l_p$, the monomer density inside the hydrodynamic screening volume decreases because the relatively narrow channel suppresses (but does not eliminate) backfolding of the chain. However, since the persistence length is much larger than the hydrodynamic radius, the chain still tends to be far enough from the wall to avoid lubrication-like flows. We thus have efficient screening of polymer-polymer hydrodynamic interactions by the walls accompanied by weak polymer-wall hydrodynamic interactions. This leads to the case where the hydrodynamic friction is, at best, a very weak function of the extension of the chain. Finally, as the channel size becomes much smaller than the persistence length, we reach a case where the walls strongly screen polymer-polymer hydrodynamic interactions but also enforce strong polymer-wall hydrodynamic interactions. This is the lubrication-like Odijk limit.

To date, there are no experimental data for the diffusion of DNA in a nanochannel as a function of the channel size that we can use to test the predictions in Fig. 6. However, we mentioned in our review of the literature that Reisner *et al.* [38] provided relaxation time data for λ-DNA in seven channel sizes ranging from 35 nm to 400 nm. We used these hydrodynamic data, in conjunction with calculations of the variance in the mean extension, to compute the relaxation time using a dumbbell model parameterized by the detailed simulations [75]. Using an $\mathcal{O}(1)$ prefactor, we were able to obtain agreement with the experimental data, which supports the picture of the hydrodynamics we described here.

Before leaving this subject, it is worthwhile to compare the case of DNA friction inside a nanochannel to the frictional force experienced by a DNA molecule during translocation through a nanopore [103–105]. The most relevant comparison is in the Odijk regime, where Eq. (32) indicates that the friction in a channel is governed by the lubrication friction between the DNA and the walls. The friction of a DNA molecule in a nanopore is also governed by lubrication flow, assuming that the dominant contribution to the friction is the chain inside the pore and not the coiled segments on either side. Thus, we would expect these two frictions to be congruent when the nanochannel approaches the $\lesssim 10$ nm range used for nanopore friction experiments [103,104]. However, it is extraordinarily difficult to operate such small nanochannels [106]. At the moment, channel widths of 45 nm seem to be the lower bound for robust routine operation [27], ableit in a commercial setting. Our results indicate that 45 nm channels are closer to the case where the hydrodynamic friction is, at best, a very weak function of the extension of the chain. Thus, the friction is qualitatively different than the lubrication limit embodied by the nanopore. Naturally, as the channel size increases further and we enter the blob regimes, the congruence between the nanopore friction and the channel friction is lost since the friction is dominated by polymer-polymer hydrodynamic interactions rather than polymer-wall hydrodynamic interactions.

5 Outlook

In this mini-review, we have focused on two results from our group pertaining to the hydrodynamics of confined DNA. Our work with Patrick Doyle [5] seems to resolve the apparent contradiction between experiments and de Gennes' blob theory for DNA in a nanoslit, where both approaches agree for the in-plane size of the confined chain but disagree for the diffusion coefficient. Indeed, extrapolating our results to higher molecular weights suggest that a Brochard-de Gennes diffusion regime with the scaling $D \sim H^{2/3}$ should be realized for DNA in the megabase pair range and micron-sized slits. The fabrication of this experimental system is much simpler than making a nanoslit, but handling such large DNA without any breakage is challenging. With respect to the nanochannel simulations [4], we think it is fair to say that the comparison between our results and experiments thus far look promising [75]. The prediction of a freely draining regime over a wide range of experiments is a strong one, running counter to the extant theories for flexible chains. However, the agreement between our simulations for the longest relaxation time of a DNA molecule in a nanochannel and experimental data [75] lend confidence to the hydrodynamic modeling. We are also optimistic that experimental data for the diffusion coefficients of channel-confined DNA will soon become available to test our predictions.

There are two natural areas of concern about our work. First, we have assumed that the pre-averaged Kirkwood approximation is a satisfactory one for a confined wormlike chain. Previous work by Jendrejack *et al.* [54] for weakly confined chains indicate that the Kirkwood pre-averaged approximation is in good agreement with the center-of-mass diffusion coefficients produced by Brownian dynamics simulations, but it remains to be seen whether this agreement holds true over the entire range of extension or for the more finely discretized models of DNA that are required for stronger confinement. Second, the results presented here are for relatively short chains, up to around 10 μm in contour length, that may not yet have reached the asymptotic limit of a long chain [98]. Thus, the data reviewed here [4, 5] may exhibit some finite length effects. We are presently working on assessing both of these open questions.

In our discussion of simulation methods, we have focused exclusively on Brownian Dynamics with hydrodynamic interactions. This is not the only possibility, and every method has intrinsic advantages and shortcomings. An alternate approach while maintaining an implicit solvent is coupling a lattice Boltzmann (LB) solution for the fluid flow to the polymer model [48, 107–112], where random fluctuations are added to the stress tensor directly [113] to introduce Brownian fluctuations. As this method solves the Boltzmann equation rather than the Stokes equation, it leads to some approximations. A rather different approach is to use discrete fluid models, which can be useful for simulating more complicated geometries where the solution to the flow field in an implicit solvent becomes difficult. We do not think that molecular dynamics (MD) approaches [114, 115] are likely to be useful here, owing to the small time steps required to capture the motion of the fluid and transmit hydrodynamics. However, it may be possible to make progress using mesoscopic, explicit fluid algorithms for confined systems, such as Dissipative Particle Dynamics (DPD) [116–118] or Multi-Particle Collision Dynamics (MPCD) [119]. Both methods have been used for modeling confined polymers [56, 120–122].

Regardless of the modeling approach, we believe that the problem of DNA dynamics in nanochannels remains a fertile area for further exploration, with important applications in biotechnology. While we have presented some preliminary ideas about the friction of a DNA chain in a square channel, most practical applications entail the use of rectangular channels due to fabrication limitations. We recently showed that the spring constant of channel-confined DNA depends in a non-trivial way on the aspect ratio of the channel [100], and it is reasonable to assume that hydrodynamic inter-

actions may also exhibit similarly peculiar behavior. It would also be worthwhile to consider other ways that the channel shape can affect the hydrodynamic interactions, either using circular channels to eliminate the corner flows or using triangular channels [123,124] to enhance the importance of these flows. Such simulations for circular confinement are driven more by curiosity, since fabrication of transparent circular nanochannels suitable for fluorescence microscopy is challenging but possible [125]. In contrast, triangular channels are easily fabricated [123,124] and provide a stronger extension than a square channel for a given cross-sectional area [126,127]. Moreover, hydrodynamic interactions may play a crucial role for the strong stretching found in "normally closed" triangular nanochannels [124]. The techniques for exploring these types of systems are now well developed and waiting to be exploited.

Our work in this area is supported by the National Science Foundation (DMR-1206045 and CBET-1262286) and the National Institutes of Health (R01-HG006851). DRT acknowledges the support of a Doctoral Dissertation Fellowship from the University of Minnesota. We thank Pat Doyle (MIT) for the fruitful collaboration discussed in this mini-review.

References

1. F. Persson, J.O. Tegenfeldt, Chem. Soc. Rev. **39**, 985 (2010)
2. W. Reisner, J.N. Pedersen, R.H. Austin, Rep. Prog. Phys. **75**, 106601 (2012)
3. K.D. Dorfman, S.B. King, D.W. Olson, J.D.P. Thomas, D.R. Tree, Chem. Rev. **113**, 2584 (2013)
4. D.R. Tree, Y. Wang, K.D. Dorfman, Phys. Rev. Lett. **108**, 228105 (2012)
5. L. Dai, D.R. Tree, J.R.C. van der Maarel, K.D. Dorfman, P.S. Doyle, Phys. Rev. Lett. **110**, 168105 (2013)
6. D. Stigter, J. Colloid Interface Sci. **53**, 296 (1975)
7. D. Stigter, Biopolymers **16**, 1435 (1977)
8. C.C. Hsieh, A. Balducci, P.S. Doyle, Nano Lett. **8**, 1683 (2008)
9. Y. Wang, D.R. Tree, K.D. Dorfman, Macromolecules **44**, 5694 (2011)
10. D.R. Tree, A. Muralidhar, P.S. Doyle, K.D. Dorfman, Macromolecules **46**, 8369 (2013)
11. C. Bustamante, J.F. Marko, E.D. Siggia, S. Smith, Science **265**, 1599 (1994)
12. N. Fakhri, F.C. MacKintosh, B. Lounis, L. Cognet, M. Pasquali, Science **330**, 1804 (2010)
13. A.V. Dobrynin, Macromolecules **39**, 9519 (2006)
14. D.E. Smith, T.T. Perkins, S. Chu, Macromolecules **29**, 1372 (1996)
15. M.L. Mansfield, J.F. Douglas, Soft Matter **9**, 8914 (2013)
16. L. Nyberg, F. Persson, B. Akerman, F. Westerlund, Nucleic Acids Res. **41**, e184 (2013)
17. D.C. Schwartz, C.R. Cantor, Cell **37**, 67 (1984)
18. R.T. Kovacic, L. Comai, A.J. Bendich, Nucleic Acids Res. **23**, 3999 (1995)
19. N. Clisby, Phys. Rev. Lett. **104**, 055702 (2010)
20. P.G. de Gennes, *Scaling Concepts in Polymer Physics* (Cornell University Press, Ithaca, NY, 1979)
21. M. Daoud, P.G. de Gennes, J. Phys. (Paris) **38**, 85 (1977)
22. T. Odijk, Macromolecules **16**, 1340 (1983)
23. D.R. Tree, W.F. Reinhart, K.D. Dorfman, Macromolecules **47**, 3672 (2014)
24. W. Reisner, J.P. Beech, N.B. Larsen, H. Flyvbjerg, A. Kristensen, J.O. Tegenfeldt, Phys. Rev. Lett. **99**, 058302 (2007)
25. K. Jo, D.M. Dhingra, T. Odijk, J.J. de Pablo, M.D. Graham, R. Runnheim, D. Forrest, D.C. Schwartz, Proc. Natl. Acad. Sci. USA **104**, 2673 (2007)
26. Y. Kim, K.S. Kim, K.L. Kounovsky, R. Chang, G.Y. Jung, J.J. de Pablo, K. Jo, D.C. Schwartz, Lab Chip **11**, 1721 (2011)
27. E.T. Lam, A. Hastie, C. Lin, D. Ehrlich, S.K. Das, M.D. Austin, P. Deshpande, H. Cao, N. Nagarajan, M. Xiao et al., Nat. Biotechnol. **30**, 771 (2012)

28. J.O. Tegenfeldt, C. Prinz, H. Cao, S. Chou, W.W. Reisner, R. Riehn, Y.M. Wang, E.C. Cox, J.C. Sturm, P. Silberzan et al., Proc. Natl. Acad. Sci. USA **101**, 10979 (2004)
29. B. Teague, M.S. Waterman, S. Goldstein, K. Potamousis, S. Zhou, S. Reslewic, D. Sarkar, A. Valouev, C. Churas, J.M. Kidd et al., Proc. Natl. Acad. Sci. USA **107**, 10848 (2010)
30. M. Xiao, A. Phong, C. Ha, T.F. Chan, D. Cai, L. Leung, E. Wan, A.L. Kistler, J.L. DeRisi, P.R. Selvin et al., Nucleic Acids Res. **35**, e16 (2007)
31. M. Levy-Sakin, Y. Ebenstein, Curr. Opin. Biotechnol. **24**, 690 (2013)
32. M. Levy-Sakin, A. Grunwald, S. Kim, N.R. Gassman, A. Gottfried, J. Antelman, Y. Kim, S.O. Ho, R. Samuel, X. Michalet et al., ACS Nano **8**, 14 (2014)
33. S.K. Das, M.D. Austin, M.C. Akana, P. Deshpande, H. Cao, M. Xiao, Nucleic Acids Res. **38**, e177 (2010)
34. A.R. Hastie, L. Dong, A. Smith, F. Finkelstein, E.T. Lam, N. Huo, H. Cao, P.Y. Kwok, K.R. Deal, J. Dvorak et al., PLoS One **8**, e55864 (2013)
35. R.L. Welch, R. Sladek, K. Dewar, W.W. Reisner, Lab Chip **12**, 3314 (2012)
36. R.B. Bird, C.F. Curtiss, R.C. Armstrong, O. Hassager, *Dynamics of Polymeric Liquids, Volume 2, Kinetic Theory*, Vol. 2 (John Wiley & Sons, Inc., 1986)
37. Y.L. Chen, M.D. Graham, J.J. de Pablo, G.C. Randall, M. Gupta, P.S. Doyle, Phys. Rev. E **70**, 060901 (2004)
38. W. Reisner, K.J. Morton, R. Riehn, Y.M. Wang, Z. Yu, M. Rosen, J.C. Sturm, S.Y. Chou, E. Frey, R.H. Austin, Phys. Rev. Lett. **94**, 196101 (2005)
39. D. Stein, F.H.J. van der Heyden, W.J.A. Koopmans, C. Dekker, Proc. Natl. Acad. Sci. USA **103**, 15853 (2006)
40. A. Balducci, P. Mao, J. Han, P.S. Doyle, Macromolecules **39**, 6273 (2006)
41. C.C. Hsieh, A. Balducci, P.S. Doyle, Macromolecules **40**, 5196 (2007)
42. P.K. Lin, C.C. Fu, Y.L. Chen, Y.R. Chen, P.K. Wei, C.H. Kuan, W.S. Fann, Phys. Rev. E **76**, 011806 (2007)
43. E.A. Strychalski, S.L. Levy, H.G. Craighead, Macromolecules **41**, 7716 (2008)
44. D.J. Bonthuis, C. Meyer, D. Stein, C. Dekker, Phys. Rev. Lett. **101**, 108303 (2008)
45. P.K. Lin, K.h. Lin, C.C. Fu, K.C. Lee, P.K. Wei, W.W. Pai, P.H. Tsao, Y.L. Chen, W.S. Fann, Macromolecules **42**, 1770 (2009)
46. J. Tang, S.L. Levy, D.W. Trahan, H.G. Craighead, P.S. Doyle, Macromolecules **43**, 7368 (2010)
47. H. Uemura, M. Ichikawa, Y. Kimura, Phys. Rev. E **81**, 051801 (2010)
48. P.K. Lin, J.F. Chang, C.H. Wei, P.H. Tsao, W.S. Fann, Y.L. Chen, Phys. Rev. E **84**, 031917 (2011)
49. F. Brochard, P.G. de Gennes, J. Chem. Phys. **67**, 52 (1977)
50. T. Odijk, Phys. Rev. E **77**, 060901(R) (2008)
51. D.W. Schaefer, J.F. Joanny, P. Pincus, Macromolecules **13**, 1280 (1980)
52. L. Dai, J.R.C. van der Maarel, P.S. Doyle, Macromolecules **47**, 2445 (2014)
53. M. Doi, S.F. Edwards, *The Theory of Polymer Dynamics* (Oxford University Press, 1986)
54. R.M. Jendrejack, D.C. Schwartz, M.D. Graham, J.J. de Pablo, J. Chem. Phys. **119**, 1165 (2003)
55. R.M. Jendrejack, D.C. Schwartz, J.J. de Pablo, M.D. Graham, J. Chem. Phys. **120**, 2513 (2004)
56. N. Watari, M. Makino, N. Kikuchi, R.G. Larson, M. Doi, J. Chem. Phys. **126**, 094902 (2007)
57. A. Izmitli, D.C. Schwartz, M.D. Graham, J.J. de Pablo, J. Chem. Phys. **128**, 085102 (2008)
58. A.P. Markesteijn, O.B. Usta, I. Ali, A.C. Balazs, J.M. Yeomans, Soft Matter **5**, 4575 (2009)
59. R. Chelakkot, R.G. Winkler, G. Gompper, Europhys. Lett. **91**, 14001 (2010)
60. J.L. Harden, M. Doi, J. Phys. Chem. **96**, 4046 (1992)
61. R.M. Jendrejack, E.T. Dimalanta, D.C. Schwartz, M.D. Graham, J.J. de Pablo, Phys. Rev. Lett. **91**, 038102 (2003)

62. H. Diamant, J. Phys. Soc. Jpn. **78**, 041002 (2009)
63. I. Pagonabarraga, M.H.J. Hagen, C.P. Lowe, D. Frenkel, Phys. Rev. E **59**, 4458 (1999)
64. B. Cui, H. Diamant, B. Lin, Phys. Rev. Lett. **89**, 188302 (2002)
65. N. Liron, S. Mochon, J. Eng. Math. **10**, 287 (1976)
66. A. Balducci, Ph.D. thesis, Massachusetts Institute of Technology (2008)
67. P. Bhattacharyya, B.J. Cherayil, J. Chem. Phys. **138**, 244904 (2013)
68. E. Werner, F. Westerlund, J.O. Tegenfeldt, B. Mehlig, Macromolecules **46**, 6644 (2013)
69. J.G. Kirkwood, J. Riseman, J. Chem. Phys. **16**, 565 (1948)
70. J.G. Kirkwood, J. Polym. Sci. **12**, 1 (1954)
71. J.J. Erpenbeck, J.G. Kirkwood, J. Chem. Phys. **29**, 909 (1958)
72. J.J. Erpenbeck, J.G. Kirkwood, J. Chem. Phys. **38**, 1023 (1963)
73. R. Zwanzig, J. Chem. Phys. **45**, 1858 (1966)
74. H. Yamakawa, *Modern Theory of Polymer Solutions* (Harper and Row, 1971)
75. D.R. Tree, Y. Wang, K.D. Dorfman, Biomicrofluidics **7**, 054118 (2013)
76. J. Rotne, S. Prager, J. Chem. Phys. **50**, 4831 (1969)
77. H. Yamakawa, J. Chem. Phys. **53**, 436 (1970)
78. W. Zylka, J. Chem. Phys. **94**, 4628 (1991)
79. R.M. Jendrejack, M.D. Graham, J.J. de Pablo, J. Chem. Phys. **113**, 2894 (2000)
80. H.C. Öttinger, *Stochastic Processes in Polymeric Fluids: Tools and Examples for Developing Simulation Algorithms* (Springer-Verlag, 1996)
81. M. Fixman, Macromolecules **19**, 1204 (1986)
82. T. Ando, E. Chow, Y. Saad, J. Skolnick, J. Chem. Phys. **137**, 064106 (2012)
83. A. Saadat, B. Khomami, J. Chem. Phys. **140**, 184903 (2014)
84. M. Fixman, J. Chem. Phys. **69**, 1527 (1978)
85. P.S. Grassia, E.J. Hinch, L.C. Nitsche, J. Fluid Mech. **282**, 373 (1995)
86. P.J. Mucha, S.Y. Tee, D.A. Weitz, B.I. Shraiman, M.P. Brenner, J. Fluid Mech. **501**, 71 (2004)
87. J.P. Hernández-Ortiz, J.J. de Pablo, M.D. Graham, J. Chem. Phys. **125**, 164906 (2006)
88. J.P. Hernández-Ortiz, J.J. de Pablo, M.D. Graham, Phys. Rev. Lett. **98**, 140602 (2007)
89. J.P. Hernández-Ortiz, P.T. Underhill, M.D. Graham, J. Phys.-Condens. Mat. **21**, 204107 (2009)
90. K.L. Kounovsky-Shafer, J.P. Hernández-Ortiz, K. Jo, T. Odijk, J.J. de Pablo, D.C. Schwartz, Macromolecules **46**, 8356 (2013)
91. M. Fixman, Macromolecules **14**, 1710 (1981)
92. B. Liu, B. Dünweg, J. Chem. Phys. **118**, 8061 (2003)
93. P. Hagerman, B. Zimm, Biopolymers **20**, 1481 (1981)
94. M. Fixman, Macromolecules **14**, 1706 (1981)
95. R. Rodríguez Schmidt, J. Hernández Cifre, J. Garcìa de la Torre, Eur. Phys. J. E **35**, 1 (2012)
96. J. Wang, H. Gao, J. Chem. Phys. **123**, 084906 (2005)
97. D.R. Tree, Y. Wang, K.D. Dorfman, Phys. Rev. Lett. **110**, 208103 (2013)
98. A. Muralidhar, D.R. Tree, Y. Wang, K.D. Dorfman, J. Chem. Phys. **140**, 084905 (2014)
99. F. Persson, P. Utko, W. Reisner, N.B. Larsen, A. Kristensen, Nano Lett. **9**, 1382 (2009)
100. D. Gupta, J. Sheats, A. Muralidhar, J.J. Miller, D.E. Huang, S. Mahshid, K.D. Dorfman, W. Reisner, J. Chem. Phys. **140**, 214901 (2014)
101. D.C. Morse, Macromolecules **31**, 7044 (1998)
102. T.W. Burkhardt, Y. Yang, G. Gompper, Phys. Rev. E **82**, 041801 (2010)
103. U.F. Keyser, B.N. Koeleman, S. van Dorp, D. Krapf, R.M.M. Smeets, S.G. Lemay, N.H. Dekker, C. Dekker, Nat. Phys. **2**, 473 (2006)
104. E.H. Trepagnier, A. Radenovic, D. Sivak, P. Geissler, J. Liphardt, Nano Lett. **7**, 2824 (2007)
105. B. Laun, A. Aksimentiev, Phys. Rev. E **78**, 021912 (2008)
106. H. Cao, Z. Yu, J. Wang, J.O. Tegenfeldt, R.H. Austin, W. Wu, S.Y. Chou, Appl. Phys. Lett. **81**, 174 (2002)
107. A. Ladd, R. Verberg, J. Stat. Phys. **104**, 1191 (2001)
108. O.B. Usta, A.J.C. Ladd, J.E. Butler, J. Chem. Phys. **122**, 094902 (2005)

109. O.B. Usta, J.E. Butler, A.J.C. Ladd, Phys. Fluids **18**, 094902 (2006)
110. Y.L. Chen, H. Ma, M.D. Graham, J.J. de Pablo, Macromolecules **40**, 5978 (2007)
111. Y.L. Chen, Biomicrofluidics **7**, 054119 (2013)
112. Y.L. Chen, Y.H. Lin, J.F. Chang, P.K. Lin, Macromolecules **47**, 1199 (2014)
113. B. Dünweg, A.J.C. Ladd, Adv. Polym. Sci. **221**, 89 (2009)
114. J.M. Polson, J.P. Gallant, J. Chem. Phys. **124**, 184905 (2006)
115. R. Khare, M.D. Graham, J.J. de Pablo, Phys. Rev. Lett. **96**, 224505 (2006)
116. P. Español, P. Warren, Europhys. Lett. **30**, 191 (1995)
117. R.D. Groot, P.B. Warren, J. Chem. Phys. **107**, 4423 (1997)
118. M. Ripoll, M.H. Ernst, P. Español, J. Chem. Phys. **115**, 7271 (2001)
119. A. Malevanets, R. Kapral, J. Chem. Phys. **110**, 8605 (1999)
120. Y. Kong, C. Manke, W. Madden, A. Schlijper, Int. J. Thermophys. **15**, 1093 (1994)
121. J. Sané, J.T. Padding, A.A. Louis, Phys. Rev. E **79**, 051402 (2009)
122. M. Chinappi, E. De Angelis, Philos. Trans. Roy. Soc. A **369**, 2329 (2011)
123. D. Huh, K.L. Mills, X. Zhu, M.A. Burns, M.D. Thouless, S. Takayama, Nat. Mater. **6**, 424 (2007)
124. K.L. Mills, D. Huh, S. Takayama, M.D. Thouless, Lab Chip **10**, 1627 (2010)
125. S. Azimi, Z. Dang, C. Zhang, J. Song, M.B.H. Breese, C.H. Sow, J.A. van Kan, J.R.C. van der Maarel, Lab Chip **14**, 2081 (2014)
126. W.F. Reinhart, D.R. Tree, K.D. Dorfman, Biomicrofluidics **7**, 024102 (2013)
127. C. Manneschi, E. Angeli, T. Ala-Nissila, L. Repetto, G. Firpo, U. Valbusa, Macromolecules **46**, 4198 (2013)